J. Biochem. 2012;151(4):423–437 doi:10.1093/jb/mvs010

JB THE JOURNAL OF BIOCHEMISTRY

Sequence requirements for RNA binding by HuR and AUF1

Received September 14, 2011; accepted December 21, 2011; published online February 25, 2012

Andrew Barker[1,2,3], Michael R. Epis[1], Corrine J. Porter[2,3,*], Benjamin R. Hopkins[3], Matthew C. J. Wilce[2,3,*], Jackie A. Wilce[2,3,*], Keith M. Giles[1] and Peter J. Leedman[1,4,†]

[1]Laboratory for Cancer Medicine, Centre for Medical Research, Western Australian Institute for Medical Research, Rear 50 Murray St., Perth, WA, 6000, Australia; [2]Pharmacology Unit, School of Medicine & Pharmacology; [3]School of Life & Chemical Sciences; and [4]School of Medicine and Pharmacology, University of Western Australia, Crawley WA 6909, Australia

[†]Peter J. Leedman, Laboratory for Cancer Medicine, WAIMR, Rear 50 Murray St., Perth, WA, 6000, Australia. Tel: +61 8 9224-0327, Fax: +61 8 9224-0322, email: peter.leedman@uwa.edu.au

*Present address: Corrine J. Porter/Matthew C.J. Wilce/ Jackie A. Wilce, Department of Biochemistry & Molecular Biology, Monash University, Clayton, Vic, 3800, Australia.

The stability of RNAs bearing AU-rich elements in their 3′-UTRs, and thus the level of expression of their protein products, is regulated by interactions with cytoplasmic RNA-binding proteins. Binding by HuR generally leads to mRNA stabilization and increased protein production, whereas binding by AUF1 isoforms generally lead to rapid degradation of the mRNA and reduced protein production. The exact nature of the interplay between these and other RNA-binding proteins remains unclear, although recent studies have shown close interactions between them and even suggested competition between the two for binding to their cognate recognition sequences. Other recent reports have suggested that the sequences recognized by the two proteins are different. We therefore performed a detailed *in vitro* analysis of the binding site(s) for HuR and AUF1 present in androgen receptor mRNA to define their exact target sequences, and show that the same sequence is contacted by both proteins. Furthermore, we analysed a proposed HuR target within the 3′-UTR of MTA1 mRNA, and show that the contacted bases lie outside of the postulated motif and are a better match to a classical ARE than the postulated motif. The defining features of these HuR binding sites are their U-richness and single strandedness.

Keywords: androgen receptor/AU-rich element/ hnRNP D/HuR/metastasis-associated protein-1/ prostate carcinoma.

Abbreviations: AR, androgen receptor; ARE, AU-rich element; AUF1, heteronuclear ribonucleic acid binding protein D (hnRNP D); BS RNA, RNA generated from the polylinker portion of plasmid pBLUESCRIPT II KS+; cFOS, human cellular homologue of Finkel-Biskis-Jinkins murine osteogenic sarcoma virus oncogene protein; FBS, fetal bovine serum; HuR, embryonic lethal abnormal vision system human homologue 1 (ELAV1); mRNA, messenger ribonucleic acid; MTA1, Metastasis-associated protein 1; REMSA, RNA electrophoretic mobility shift assay; RRM, RNA-recognition motif; 3′-UTR, 3′-untranslated region.

Over the past decade, post-transcriptional events, including messenger ribonucleic acid (mRNA) export, stability and translation efficiency have emerged as critical steps in the regulation of gene expression in mammals. In particular, many cytokine and proto-oncogene mRNAs have been identified as containing AU-rich elements (AREs) within their 3′-UTRs, which confer a short half-life on the mRNAs (*1*). ARE elements function primarily as the binding sites for a number of discrete RNA-binding proteins, the most extensively studied of which are the ubiquitously expressed HuR (embryonic lethal abnormal vision system human homologue 1 (ELAV1)) and isoforms of AUF1 (heteronuclear ribonucleic acid binding protein D (hnRNP D)). Cytoplasmic binding of HuR to ARE-containing mRNAs is generally accepted to lead to stabilization, whereas the effects of AUF1 are complicated in that the conferring of either stabilization or destabilization depend on both the cell type and the AUF1 isoform involved (*2–4*).

Unlike the closely related HuB, HuC and HuD, which are abundant only in neural tissue, HuR is ubiquitously expressed in mammalian tissues (*5*, *6*), and although predominantly located in cell nuclei (≥90% of the total), transient shuttling between nucleus and cytoplasm does occur (*7–9*). HuR contains three RNA recognition motifs (RRMs), with a long hinge region that includes the domain responsible for nuclear/cytoplasmic shuttling (*7*), separating the second and the third RRM. Phosphorylation of serine residues within this hinge region influences subcellular localization of HuR, with phosphorylation of S202 or S242 leading to the accumulation of HuR in the nucleus (*10*, *11*). The first two RRM domains mediate recognition of U-rich target RNA sequences (*12–15*), whereas the third RRM, originally implicated in binding poly-A tails of mRNAs (*16*), has recently been shown to mediate 3′-terminal adenosylation of non-polyadenylated RNA (*17*).

The four AUF1 isoforms all contain two RRM domains in the central portion of the protein, with differences between isoforms occurring at both N- and C-termini through alternative splicing of the primary transcript (*18*). Like HuR, AUF1 isoforms also undergo nucleo-cytoplasmic shuttling, although at least some of the sequences facilitating nuclear import or export appear to be isoform specific (*19*).

Again, nucleo-cytoplasmic shuttling appears to be modulated by phosphorylation (*20*). As AUF1 binding generally leads to mRNA destabilization, it is not surprising that HuR and AUF1 can compete for binding to a number of mRNAs (*21*). More recently, co-localization and functional interactions between HuR and AUF1 have been demonstrated in both the nucleus and cytoplasm (*22*).

The best characterized RNA target sequence bound by HuR and AUF1 is the ARE, divided into three classes, and found in the 3′-UTR of diverse mRNAs (*23*, *24*). Recognition of AREs by HuR is dependent on their presence within a single-stranded stretch of RNA (*25*). ARE-containing mRNAs typically encode cytokines or proto-oncogenes, and generally have short half-lives. A variety of stimulatory signals leads to an increase in cytoplasmic concentration of HuR, which then leads to the stabilization of ARE-containing mRNAs and a much more rapid increase in the gene product than would be possible with alterations in gene transcription rates (*26–32*). Cytoplasmic HuR also plays a role in the normal development (*33–35*), as well as featuring in a number of malignancies, including breast, ovarian and prostate carcinomas (*36–38*), although the nuclear export pathways followed by HuR appear to differ between normal and malignant tissues (*39*). HuR has been implicated in the increased production of androgen receptor (AR) in prostate carcinomas (*40*), and cytoplasmic accumulation of HuR can result from treatment of Jurkat cells with dihydrotestosterone (*41*) or of MCF7 cells with tamoxifen (*36*), whereas cytoplasmic accumulation of some AUF1 isoforms occurs upon oestrogen treatment of ovariectomized rat uterus (*42*) and is influenced by testosterone levels in mice (*43*). Array-based approaches have indicated that the total number of mRNAs bound by both proteins is large (*44–46*).

Target motifs for HuR and AUF1 have been proposed on the basis of computational analyses of RNA sequences co-immunoprecipitated by an anti-HuR antibody from RKO cells (*44*) or by an anti-AUF1 antibody from HeLa cells (*46*). The derived consensus sequence, however, bears little resemblance to the widely accepted ARE motif (*23*, *24*), nor does it resemble a UC-rich sequence bound by HuR in the 3′-UTR of AR mRNA (*40*); nor do the two motifs closely resemble each other (Fig. 1A), a surprising result given the strong suggestion for competition for binding to target RNA between the two proteins (*21*, *22*). We therefore undertook a detailed analysis of HuR and AUF1 binding to ARE and UC-rich binding sites, and in addition conducted further analysis of the sequence contacted by HuR in the 3′-UTR of metastasis-associated protein 1 (MTA1).

Materials and Methods

Plasmids, bacterial culture and cell culture

Plasmids coding full-length HuR (residues 2–326), the first two RRM domains of HuR (residues 2–188; indicated throughout as $HuR_{I\&II}$) and the third RRM domain of HuR (residues 241–326; indicated throughout as HuR_{III}) as GST fusions are described elsewhere (*40*). Full-length AUF1 p37 (residues 2–287) was amplified from plasmid pBAD/HisB-p37AUF1 (*47*) with PCR primers 5′-GGGGGGGGATCCCGAGGAGCAGTTCGGCGG and 5′-GGGGGGGAATTCGCACCTGTTGGGGATAAGT. After digestion with BamHI and EcoRI, the resulting fragment was cloned into similarly digested pGEX6P2 (GE Healthcare, Little Chalfont, UK). Target RNA sequences (AR, nucleotides 3,275–3,325 of NCBI nucleotide data base accession number M20132; MTA1, nucleotides 2,462–2,540 of accession number NM_004689) were cloned between the BamHI and HindIII sites of pBluescript II KS^+ from Stratagene (Agilent Technologies, Santa Clara, CA, USA) as complementary, synthetic DNA oligonucleotides purchased from Geneworks (Adelaide, SA, Australia). Where applicable, these sequences were also excised as SpeI–ApaI fragments and cloned between the SpeI and ApaI sites of pGL3-MCS (*48*). *Escherichia coli* DH5α was used for recombinant DNA manipulations and for purification of plasmid DNA, whereas *E. coli* BL21 Codon + (RP) from Novagen (Merck KGaA, Darmstadt, Germany) was used for over-expression of GST-fusion proteins prior to purification. Growth media in all cases was Luria-Bertani Medium (LB broth) (*49*). The human prostate carcinoma cell lines 22Rv1 and LNCaP were obtained from American Tissue Culture Collection, and were maintained in Roswell Park Memorial Institute Medium 1,640 supplemented with 10% foetal bovine serum (FBS). Cells were maintained for a maximum of 20 passages.

Protein purification

HuR, $HuR_{I\&II}$ and HuR_{III} were over-expressed as GST fusion proteins and purified essentially as described previously (*40*), except for the use of 0.5% (w/v) cholic acid instead of 0.5% Triton X-100 in cation-exchange buffers. AUF1 p37 was purified by similar methodology, except that the removal of the GST portion of the fusion protein was by PreScission protease (GE Healthcare) cleavage. Protein concentrations were determined from A_{280} of dilutions using the appropriate theoretical extinction coefficient (HuR, $\varepsilon_o = 24{,}180\,M^{-1}cm^{-1}$; $HuR_{I\&II}$, $\varepsilon_o = 7{,}680\,M^{-1}cm^{-1}$; HuR_{III}, $\varepsilon_o = 15{,}340\,M^{-1}cm^{-1}$; AUF1 p37 $\varepsilon_o = 20{,}460\,M^{-1}cm^{-1}$) (*50*) and ranged from 0.25 to 1.2 mM. All proteins migrated as single bands of expected molecular weight on SDS–PAGE gels, and preliminary gel filtration experiments indicated all were monomeric in solution (data not shown). Mass spectrometry (Proteomics International, Perth, WA, Australia) gave mass determinations within 1 Da of masses predicted from protein sequence for all full-length proteins (data not shown).

Preparation of RNA target sequences

Plasmid templates containing target sequences were linearized with HindIII or Acc65I for *in vitro* transcription reactions with T7 RNA polymerase using MEGAshortscript™ kits by Ambion (Life Technologies, Carlsbad, CA, USA) according to the manufacturer's instructions. Full-length RNAs were isolated by electrophoresis on denaturing acrylamide gels, located by UV shadowing and eluted into 15 mM NaCl, 1.5 mM Na_3 citrate, 200 mM Na acetate pH 7.0 overnight at 4°C prior to recovery. For RNA electrophoretic mobility shift assay (REMSA) and RNase footprint experiments, all RNAs were 5′-end-labelled using $\gamma[^{32}P]$ ATP from Perkin Elmer (Waltham, MA, USA) and T4 polynucleotide kinase (KinaseMax™, Ambion) according to manufacturer's instructions and then purified by denaturing gel electrophoresis (full-length targets being located by brief autoradiography) and elution as above. RNA secondary structure predictions were performed using Mfold (*51*).

RNA–protein interaction assays: REMSA and RNase footprint

Purified proteins were diluted to 2× final concentration in 1× binding buffer [10 mM HEPES pH 7.5, 3 mM $MgCl_2$, 14 mM KCl, 5% (v/v) glycerol, 0.2% (v/v) Nonidet NP-40, 50 μg/ml BSA, 1 mM DTT] immediately before use. Target RNAs (in H_2O) were heated for 10 min at 75°C then quenched on ice prior to dilution to 4× final concentration (in H_2O) and the addition of an equal volume of 2× binding buffer immediately prior to use. Diluted protein and RNA were mixed (final volume = 10 μl) and incubated at room temperature for 30 min. A quantity of 4 μl of loading buffer [1× binding buffer also containing 50% (v/v) glycerol and 0.04% (w/v) each bromophenol blue and xylene cyanol] was added and the mixture immediately loaded onto non-denaturing PAGE gels (*52*). Apparent K_d values for protein–RNA binding were calculated by non-linear regression from binding curves obtained from a

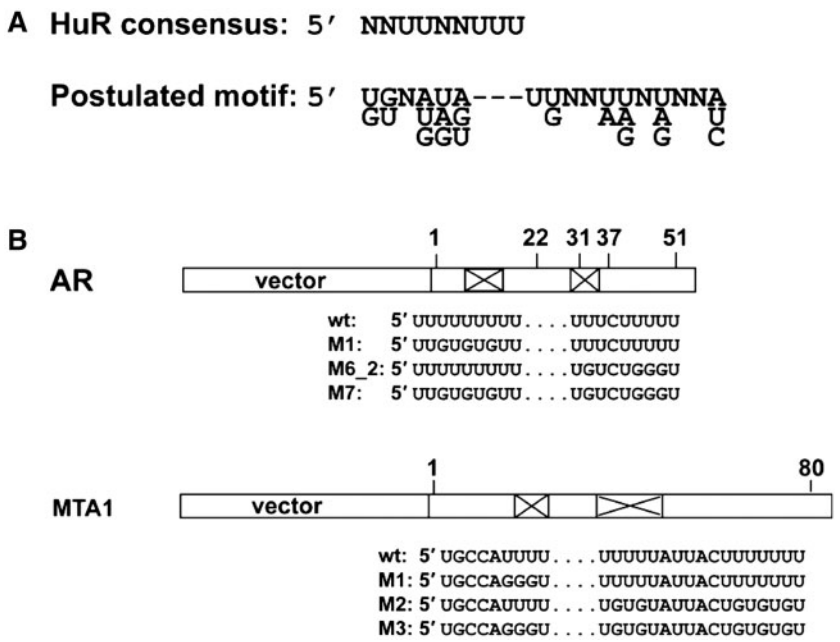

Fig. 1 Sequence motifs analysed in this study. (A) The minimal, consensus HuR binding site contained in the widely accepted ARE motif (*23*, *24*), labelled as such, is shown at the top. Underneath, the alternative postulated binding motif for HuR (derived from ref. *44*) is shown. In the latter schematic, the upper-most base represents the most probable base at that position while the bases underneath indicate bases that occur with lower frequency at the position in question. The reader is directed to ref. (*44*) for a full explanation. (B) Schematic view of target RNAs used. The 51 nt in the 3′-UTR of AR or the 79 nt in the 3′-UTR of MTA1 are depicted in cartoon form. The proximal part of the target RNAs is derived from vector sequence, and is labelled 'vector' to indicate this. The distal portions represent 51 nt from AR 3′-UTR or 80 nt from MTA1 3′-UTR, respectively. Crossed boxes within the target sequence indicate the position of introduced mutations, and the relevant sequences are shown below each cartoon. Numbers above the cartoons indicate the end-points of the insert sequences, whereas the end-points of deletion mutations within the AR target sequence are also indicated by numbers above the cartoon. Target RNAs containing the 27 nt cFOS ARE or the 38 nt TNFα ARE are of similar form (data not shown). The full RNA sequence of all target RNAs is shown in Supplementary Fig. S1.

minimum of three independent experiments using Prism 5.03 software (GraphPad Software Inc. La Jolla, CA, USA). To avoid complications with the multiple binding sites apparent for some target RNAs (see Results section), binding was assumed to be a single bi-molecular interaction and percent-bound RNA was calculated from the relationship Bound RNA = 1 − Free RNA (compared with total input RNA). Note that this possibly over-estimates K_d for complexes where the calculated K_d is close to the concentration of input RNA (10 nM). For RNase footprint reactions, protein and RNA were treated identically, except that binding reactions were in a total volume of 60 µl. After incubation as above, 10 µl of the mixture was removed for REMSA. RNase footprint reactions were performed by removing 10 µl aliquots of the binding reaction and mixing with 1 µl of each of RNaseA, RNaseT_1, RNase1 or RNaseV_1 (Ambion)—diluted in H_2O to a concentration pre-determined in pilot experiments to give an appropriate digestion pattern—and incubated for 15 min at room temperature. Proteinase K and SDS were then added to a final concentration of 0.25 µg and 0.05% (w/v), respectively, in a total volume of 100 µl and the mixture incubated for 15 min at room temperature, prior to extraction with phenol/chloroform/isoamyl alcohol (25/24/1) and precipitation of RNA from the aqueous phase. Pellets were resuspended in 7 µl formamide/dye (Ambion) prior to electrophoresis of half on high-resolution sequence gels. 'Untreated' negative control RNAs were incubated with 1 µl H_2O and handled in an otherwise identical manner. RNA ladders were generated by incubating 5′-end-labelled RNA with 0.1 µg yeast tRNA in a total volume of 5 µl 50 mM NaCarbonate pH 9.2, 1 mM EDTA at 95°C for 3–10 min (the appropriate time being determined in preliminary experiments), then quenching on ice. A quantity of 10 µl formamide/dye (as above) was added to the mixture prior to electrophoresis of 5 µl of the total. After electrophoresis, for both REMSA and RNase footprint experiments, gels were dried and exposed to phosphorimager plates.

Transient transfections and luciferase reporter assays

Firefly luciferase reporter plasmids with the relevant target RNA sequence cloned between the SpeI and ApaI site within the 3′-UTR (*48*) were transiently transfected into 22Rv1 or LNCaP cells in triplicate. Firefly luciferase assays (normalized for transfection efficiency to co-transfected *Renilla* luciferase) were performed using the Promega (Madison, WI, USA) Dual-Luciferase reporter assay system according to manufacturer's instructions.

Results

High affinity HuR binding sites are contacted by multimers of HuR

We first focused on three well-defined HuR target sequences, derived from the 3′-UTRs of AR, human cellular homologue of Finkel–Biskis–Jinkins murine osteogenic sarcoma virus oncogene protein (cFOS) and tumour necrosis factor α (TNFα) mRNAs (*40*). A schematic of the AR and MTA1 target probes, including the positions of mutations within these probes, is shown in Fig. 1B, whereas the full sequence of all RNA probes used is shown in Supplementary Data (Supplementary Fig. S1). We examined binding by both full-length HuR and a truncated variant $HuR_{I\&II}$ (that lacks the hinge region and the third RRM domain of full-length HuR) for which the structural information is available (*15*) to ensure that both proteins are binding to the same target sequence. As shown in Fig. 2, purified HuR and $HuR_{I\&II}$ (that lacks the hinge region and the third RRM domain) binds to each of these with roughly similar affinity in REMSA (Table I). The apparent K_d values obtained from these experiments are similar to previously published results (*22*). An immediate question raised by the retardation

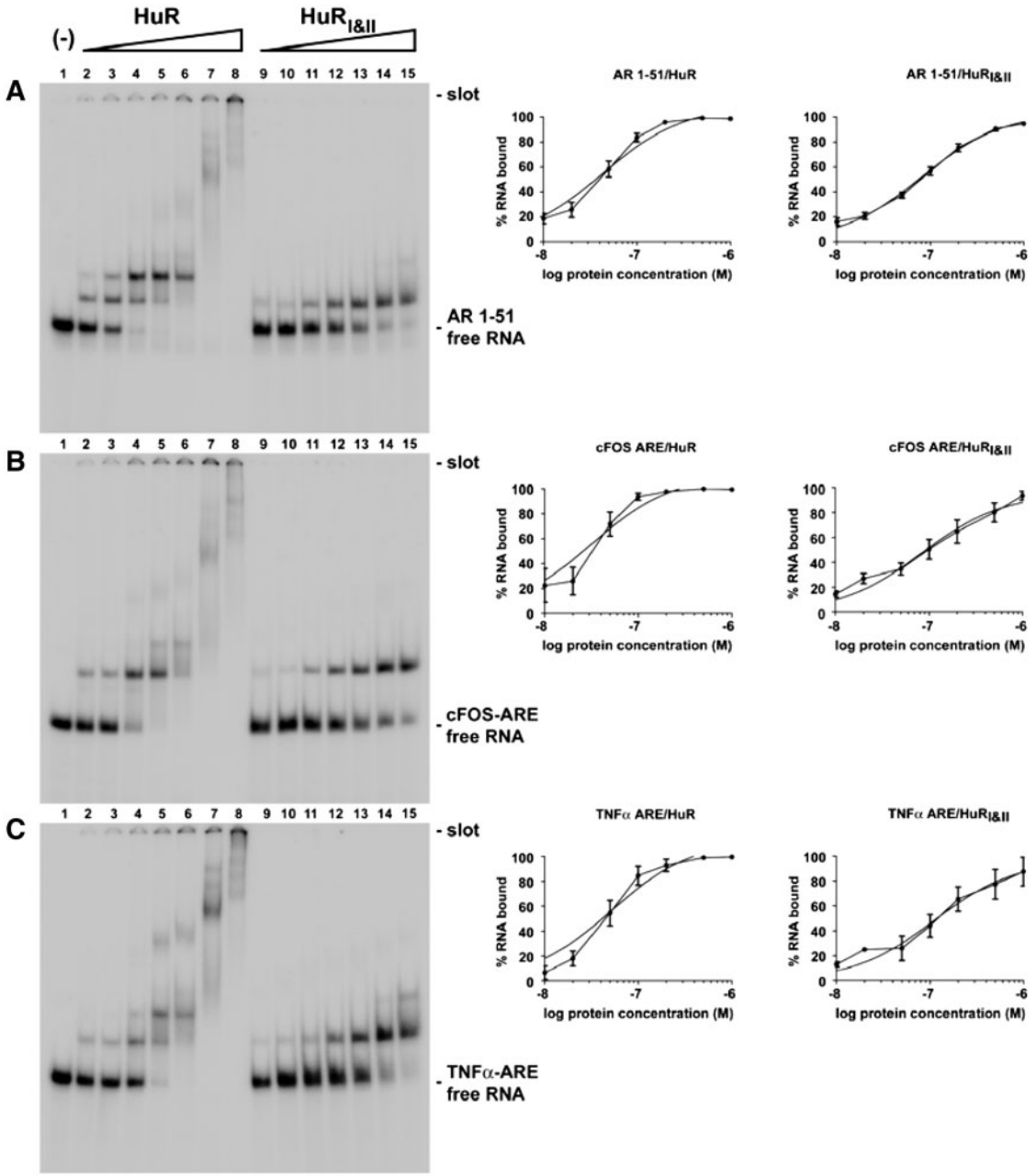

Fig. 2 HuR and HuR$_{I\&II}$ bind with high affinity to AR 1–51, cFOS-ARE and TNFα-ARE target sequences. REMSA gels are shown in which HuR or HuR$_{I\&II}$ interact with: (A) AR 1–51; (B) cFOS-ARE; or (C) TNFα-ARE. Target sequences are shown in Supplementary Fig. S1. Numbering above each gel indicates the lanes. The binding reaction for lane 1 contained no protein. Binding reactions for lanes 2–8 contained: 1×10^{-8} M, 2×10^{-8} M, 5×10^{-8} M, 1×10^{-7} M, 2×10^{-7} M, 5×10^{-7} M, or 1×10^{-6} M HuR (calculated per monomer), respectively. Binding reactions for lanes 9–15 contained equivalent amounts of HuR$_{I\&II}$ as lanes 2–8 of HuR. All binding reactions contained 1×10^{-8} M of the relevant target RNA. (−) indicates the absence of protein, whereas the wedges labelled with 'HuR' or 'HuR$_{I\&II}$' indicate increasing concentrations of each protein above the other lanes. The positions of the free RNA (unbound) and slot (origin) are indicated to the right of each gel. Binding curves to the right of each gel show input protein concentration versus bound RNA and are the plots generated by GraphPad Prism for determination of K_d as described in 'Materials and Methods' section.

Table I. Apparent K_d values for the initial binding of HuR or HuR$_{I\&II}$ to AR 1–51, cFOS-ARE or TNFα-ARE target RNAs shown in Fig. 2.

	K_d (nM)	
Target RNA	**HuR**	**HuR$_{I\&II}$**
AR 1–51	43 ± 5	81 ± 7
cFOS-ARE	26 ± 16	86 ± 34
TNFα-ARE	52 ± 23	150 ± 30

pattern seen in these gels concerns the stoichiometry of the observed complexes. By comparing the relative mobility of the predominant retarded band seen with HuR$_{I\&II}$ (MW ~20,000 Da) with the mobility of the predominant retarded band seen with full-length HuR (MW ~38,000 Da), noting the 1:1 stoichiometry of the homologous HuD$_{I\&II}$:cFOS 11-mer crystal structure (*15*), and assuming a similar RNA conformation for the two complexes suggests that the first retarded

complex contains one monomer of HuR, or two monomers of $HuR_{I\&II}$, or multiples thereof (Fig. 2). For HuR, higher order complexes are also visible (Fig. 2, lanes 7 and 8). These results are strikingly similar to those presented for *Drosophila* embryonic lethal abnormal visual system (ELAV) binding to conserved AU4-6 motifs (*53*). In contrast to the result with $HuR_{I\&II}$, binding by the purified third RRM domain of HuR, HuR_{III}, was not observed: to the target RNAs used here; to poly-adenylated versions; nor to other A-rich target sequences (data not shown).

Unlike the cFOS-ARE and TNFα-ARE, the AR 1–51 sequence has a pronounced asymmetry, in terms of the distribution of uracils throughout the sequence. We therefore concentrated on this sequence for the next series of experiments. Binding of HuR and $HuR_{I\&II}$ to the site-specific mutant targets AR 1–51 M1 (within the region from bases 7 to 15) or AR 1–51 M6_2 (within the region from bases 27 to 35) is significantly reduced, whereas only residual binding of both proteins is observed to the combination mutation AR 1–51 M7 (Fig. 3 and Table II). This result is supported by the analysis of binding by HuR and $HuR_{I\&II}$ to deletion mutations extending from either the 5′- or 3′-end. Again, the presence of two high-affinity sites for HuR is indicated: one in the region from bases 1 to 22, the other in the region from bases 22 to 37 within the AR 1–51 sequence, each of which is apparently contacted by one monomer of HuR or two monomers of $HuR_{I\&II}$ (Fig. 4 and Table III). It is interesting to note that the effects of substitution or deletion mutations are comparable: complexes between HuR and AR 1–51 M1 or AR 22–51 show the same K_d; AR 1–51 M6_2 and AR 1–22/AR 1–31 also give similar K_d values (Tables II and III).

We next examined binding by HuR and $HuR_{I\&II}$ to AR 1–51, cFOS-ARE and TNFα-ARE targets in RNase footprinting assays. Given the lack of target asymmetry mentioned above, footprints of HuR- or $HuR_{I\&II}$-bound cFOS-ARE or TNFα-ARE did not indicate a preferred portion of the ARE element for single occupancy by HuR; rather the footprint shows a gradual protection of the entire ARE sequence (Supplementary Fig. S2). As expected, given the pronounced target sequence asymmetry, similar assays performed with AR 1–51 were much more informative (Fig. 5). At the lowest HuR concentration examined, the HuR (partial) footprint with RNaseA (cleaves after pyrimidines) or RNase1 (cleaves preferably after non-base paired residues) is confined to eight out of nine contiguous uracils (bases 6–15 in the AR 1–51 sequence) in the proximal portion of the target sequence (lanes 4 and 18). This sequence is also the only sequence significantly protected from digestion in the presence of $HuR_{I\&II}$ (lanes 7–9 and 21–23). At higher HuR concentrations, a second protected region becomes apparent commencing at U28 (lanes 5 and 19), although the distal end of this second binding site cannot be assigned due to a lack of digestion of the four bases distal to U32. Weak protection of bases in this region is also apparent with the highest concentration of $HuR_{I\&II}$ (most apparent with RNase1 in lane 23). At the highest HuR concentration examined,

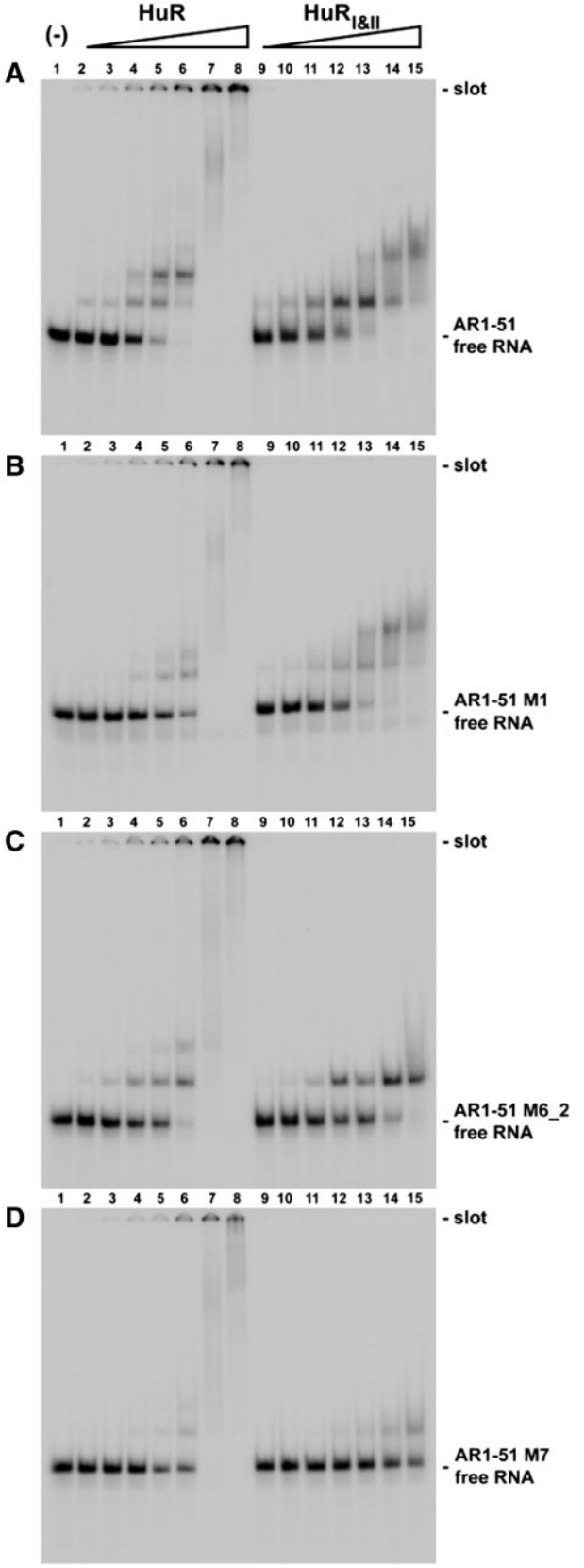

Fig. 3 Mutations within the AR 1–51 target RNA affect HuR binding. REMSA gels are shown in which HuR or $HuR_{I\&II}$ interact with: (A) AR 1–51; (B) AR 1–51 M1; (C) AR 1–51 M6_2; or (D) AR 1–51 M7. Labelling of the gels and concentrations of HuR, $HuR_{I\&II}$ and target RNAs is the same as in Fig. 2. Note that the gel shown in (A) is an independent replicate of Fig. 2A.

Table II. Apparent K_d values for the initial binding of HuR or $HuR_{I\&II}$ to AR 1–51 or target RNAs with substitution mutations shown in Fig. 3.

	K_d (nM)	
Target RNA	**HuR**	**$HuR_{I\&II}$**
AR 1–51[a]	43 ± 5	81 ± 7
AR 1–51 M1	320 ± 100	130 ± 20
AR 1–51 M6_2	160 ± 30	140 ± 20
AR 1–51 M7	>1,000	>1,000

[a]This value is taken from Table 1.

protection against RNaseA or RNase1 digestion extends outside of the minimal protected regions, presumably reflecting the presence of unspecific protein–RNA complexes at this concentration (lanes 6 and 20). The lack of digestion with $RNaseT_1$ (cleaves after Gs) within the protected region is due to the absence of guanine residues within this sequence, while the lack of $RNaseV_1$ (cleaves preferably after base-paired residues) digestion within the distal, non-vector derived sequences shown, reflect their relative single strandedness under the experimental

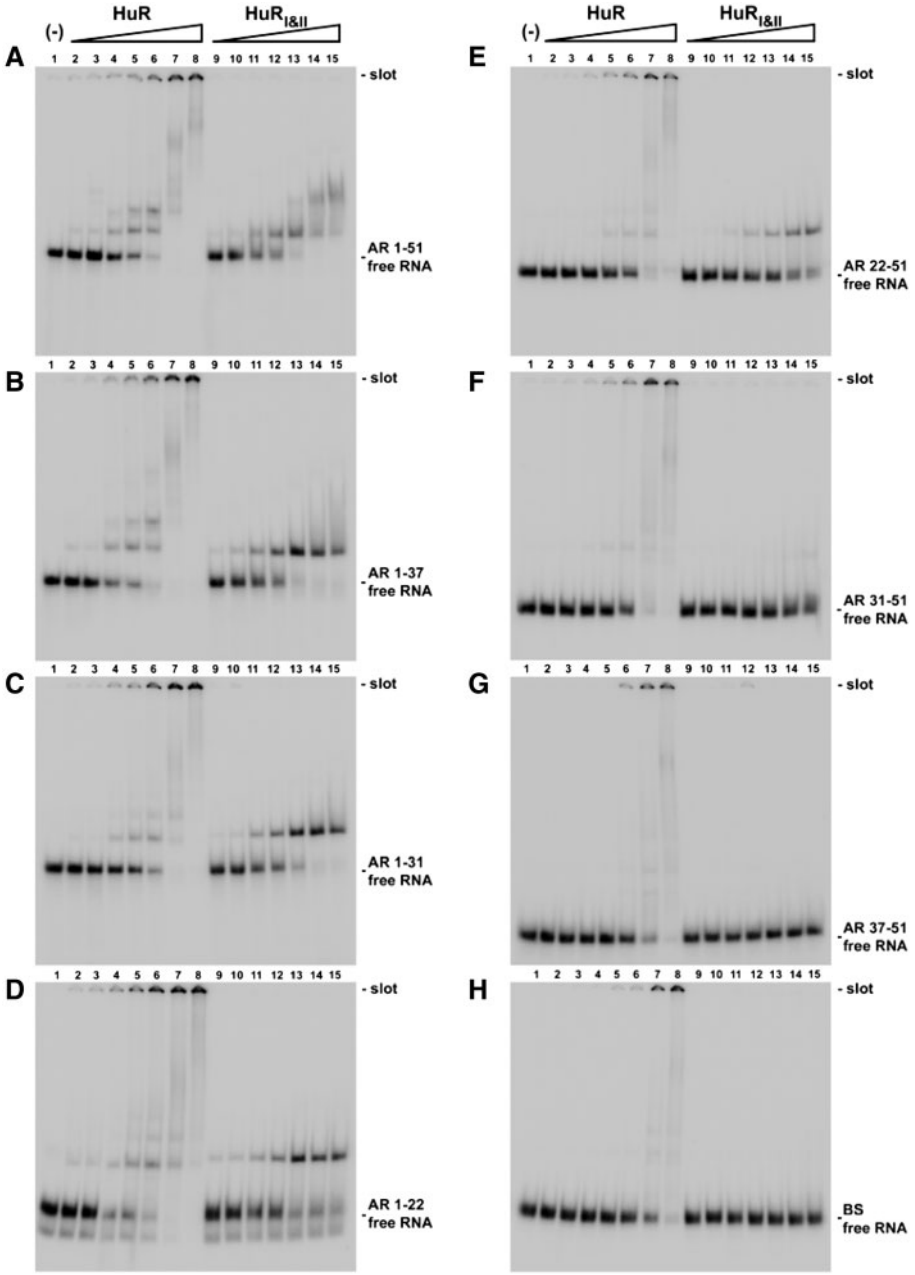

Fig. 4 HuR and $HuR_{I\&II}$ binding sites within the AR 1–51 target RNA as defined by deletions extending from the 5′- or 3′-end. REMSA gels are shown in which HuR or $HuR_{I\&II}$ interact with: (A) AR 1–51; (B) AR 1–37; (C) AR 1–31; (D) AR 1–22; (E) AR 22–51; (F) AR 31–51; or (G) AR 37–51. (H) HuR or $HuR_{I\&II}$ interactions with a target RNA derived from the empty vector (a T7 transcript derived from pBluescript II KS+ linearized with HindIII; BS in Supplementary Fig. S1) is shown. Nucleotides still present in the deletion mutants are indicated for the target sequences used in (A–G) Fig. 1. For example, nucleotides 38–51 are deleted in AR 1–37 and nucleotides 1–36 are deleted in AR 37–51. Labelling of the gels and concentrations of HuR, $HuR_{I\&II}$ and target RNAs is the same as in Fig. 2 (see legend for details). Note that the gel shown in (A) is an independent replicate of Fig. 2A.

Table III. Apparent K_d values for the initial binding of HuR or $HuR_{I\&II}$ to AR 1–51 or target RNAs with deletion mutations, or negative control (BS) target RNA, shown in Fig. 4.

	K_d (nM)	
Target RNA	**HuR**	**$HuR_{I\&II}$**
AR 1–51[a]	43 ± 5	81 ± 7
AR 1–22	190 ± 40	350 ± 50
AR 1–31	99 ± 15	100 ± 10
AR 1–37	58 ± 9	75 ± 9
AR 22–51	300 ± 80	130 ± 40
AR 31–51	590 ± 230	>1,000
AR 37–51	>1,000	>1,000
BS	>1,000	>1,000

[a]This value is taken from Table I.

conditions used. Secondary structure predictions (*51*) also suggest the contacted region is predominantly single stranded in the target RNA, as well as in the AR 3′-UTR (data not shown).

AUF1 p37 binds to the same sequence as HuR in the AR 3′-UTR

We next examined binding of purified AUF1 to the same target RNAs evaluated for HuR binding in Fig. 2 in REMSA. Significant binding of AUF1 p37 was observed with all targets, including negative control RNAs in the absence of competitor tRNA (Fig. 6). Pre-incubation of AUF1 p37 with competitor tRNA led to a decrease in the apparent binding, although a residual retarded band was still apparent at ≥20-fold molar excess of protein for BS RNA (Fig. 6A), and retarded bands possibly corresponding to monomer, dimer and tetramer complexes (*54*) are observed with the other three target RNAs (Fig. 6B–D). Evaluation of the apparent K_d of the complexes observed in the presence of competitor tRNA (Table IV) confirms that specific binding is of higher affinity to the cFOS-ARE than the other two targets. Competition between AUF1 p37 and HuR for binding to cFOS-ARE has been demonstrated (*22*) and the two proteins show roughly equivalent affinities for that target (Tables I and IV) (*22*). As AUF1 p37 binding to AR 1–51 is ~5-fold weaker than HuR (Tables I and IV), we did not attempt a comparable analysis for this target RNA. We nevertheless examined its binding to AR 1–51 in RNase footprinting assays (Fig. 7). Although a broader protein concentration range was used here than above (Fig. 5), HuR protected the same eight contiguous Us as previously from digestion with RNaseA, and the entire insert sequence is protected from digestion at the higher protein concentrations used here with both RNaseA and RNase1 (highest concentration being 10^{-6} M here as opposed to 10^{-7} M in Fig. 5). As AUF1 p37 binding is considerably weaker under these experimental conditions, protection is observed from RNaseA or RNase1 digestion only at the highest protein concentration, but the same eight Us are protected as are protected by HuR binding. The absence of Gs in the bound sequence is consistent with the lack of RNaseT1 digestion, although some hypersensitivity to RNaseT1 digestion is apparent at the highest HuR concentration at the extreme 3′-end of the probe (these extra sequences are not present in the target RNA used in the gel shown in Fig. 5). Some differences in the digestion pattern obtained with RNaseV1 between Figs 5 and 7 are also apparent. While almost no digestion of the predominantly single-stranded target RNA was evident with RNaseV1 in Fig. 5, significant digestion, as well as protection from this digestion by increasing concentrations of both HuR and AUF1 p37, was seen (Fig. 7). This is due to the presence of competitor tRNA in the latter experiment that resulted in a 1,000-fold higher concentration of RNaseV1 being required for any target digestion compared with the experiment shown in Fig 5. The resulting digestion pattern is thus most unlikely to reflect the base pairing of the digested RNA.

The actual HuR motif is close to, but not within, the predicted motif for MTA1

The features defined for the HuR binding site in AR 1–51 above—U richness, tolerance of Cs but not Gs and single strandedness, are all at variance with a postulated HuR motif (*44*). We therefore investigated whether the predicted motif might lie close to genuine HuR binding sites in the mRNAs identified. Examination of secondary structure predictions of the 3′-UTRs for several predicted HuR sites (see Fig. 2 in Ref. *44*) showed that in all cases, the predicted motif was flanked (within 30 bases) by a U-rich and at least partially non-base paired region in RNA secondary structure predictions (*51*). For subsequent analysis, we focused on the HuR site in MTA1, as (unlike other analysed sequences) our alternative motif lies within the same single stem–loop of the most energetically favourable structure prediction for the folded 3′-UTR. As the introduction of Gs within U-rich sequences contacted by HuR clearly dramatically reduces binding affinity (Fig. 3 and Table II), we designed three mutant MTA1 targets as well: M1 should disrupt binding if the predicted motif (*44*) is correct; M2 should disrupt binding to our alternative motif; while M3 is a combination of the two (Fig. 1B and Supplementary Fig. S1).

We first introduced our MTA1 target sequence and mutants (along with the AR 1–51 target sequence and mutants for comparison) into the 3′-UTR of firefly luciferase reporter vectors. In transient transfection of 22Rv1 or LNCaP cells, neither target sequence nor any of the mutations led to significant alterations in luciferase expression (Supplementary Fig. S3). Therefore, we examined HuR (and $HuR_{I\&II}$) binding to the same MTA1 target RNAs in REMSA. The MTA1 probe is bound by both proteins and in a manner indicating the presence of two binding sites for HuR monomers (Fig. 8A). The mutations introduced in MTA1 M1 have no effect on the affinity or stoichiometry of HuR or $HuR_{I\&II}$ binding (Fig. 8B), while the mutations introduced in MTA1 M2 (and M3) have a significant effect on both affinity (Table V) and stoichiometry of HuR binding, but a lesser effect on binding by $HuR_{I\&II}$ (Fig. 8C and D).

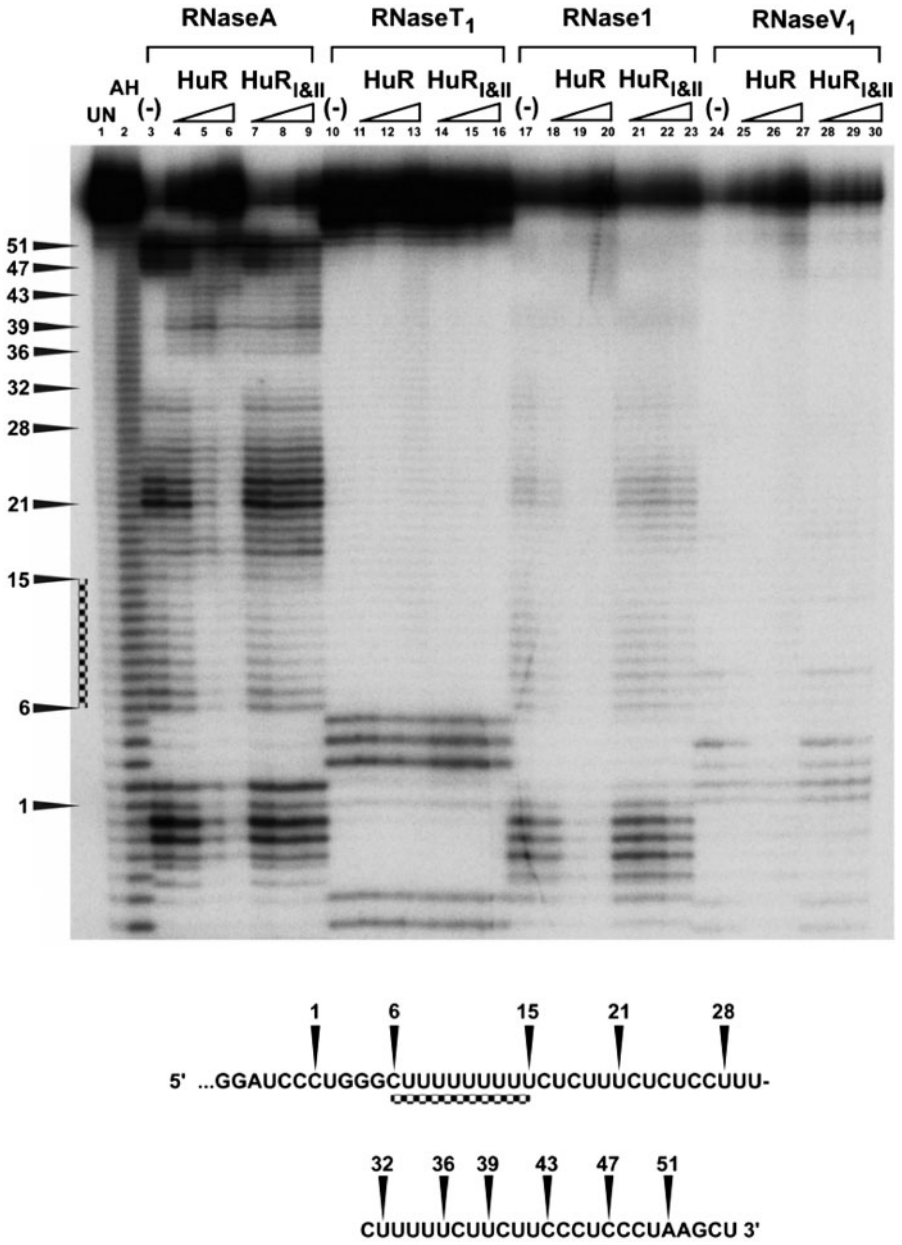

Fig. 5 RNase footprint analysis of HuR binding to AR 1–51 target RNA. Lane 1 contains 'untreated' AR 1–51 RNA (see Materials and Methods section) and is also labelled 'UN'. Lane 2 contains AR 1–51 RNA subjected to partial alkaline hydrolysis in order to generate a ladder corresponding to consecutive bases and is also labelled 'AH'. Lanes 3–9 are partially digested with RNaseA (which cleaves after Us or Cs) and binding reactions contain: 3, no protein; 4, 5×10^{-8} M HuR; 5, 1×10^{-7} M HuR; 6, 2×10^{-7} M HuR; 7, 5×10^{-8} M $HuR_{I\&II}$; 8, 1×10^{-7} M $HuR_{I\&II}$; or 9, 2×10^{-7} M $HuR_{I\&II}$. The presence or absence of protein is indicated as previously. RNaseA digestion is also indicated by a label above lanes 3–9. Lanes 10–16 are $RNaseT_1$-digested (which cleaves after Gs); lanes 17–23 are RNase1 digested (which cleaves preferentially after non-base paired residues); and lanes 24–30 are $RNaseV_1$ digested (which cleaves preferentially after base paired residues). Bands in the gel are assigned to the AR 1–51 target RNA sequence below the gel by numbering, and the bases protected by the lowest concentrations of HuR or $HuR_{I\&II}$ are indicated by dashed lines.

In order to confirm the region within the MTA1 probe bound by HuR and $HuR_{I\&II}$, we performed RNase footprint assays. As shown in Fig. 9, the MTA1 target sequence shows sufficient asymmetry for the unambiguous assignment of bases to two regions within the sequence. At the lowest HuR concentration, RNase1 digestion gives a partial HuR footprint that indicates that the Us (and single A) from U28 to U37 form the primary HuR binding site (Fig. 9, lane18). This sequence is also protected by $HuR_{I\&II}$ (lanes 21–23). At higher HuR concentrations, the protected region extends 3′ to this, covering the rest of the U-rich region up to U49 (lanes 19 and 20) and at the highest concentration also extends 5′ into the Us that form the distal portion of the binding site predicted previously (lane 20). These observations, whichdo not involve the predicted motif (*44*), are reinforced by RNaseT1 digestion, which shows an increasing hypersensitivity for G14, G15 and G17 with increasing amounts of HuR (lanes 11–13), a region

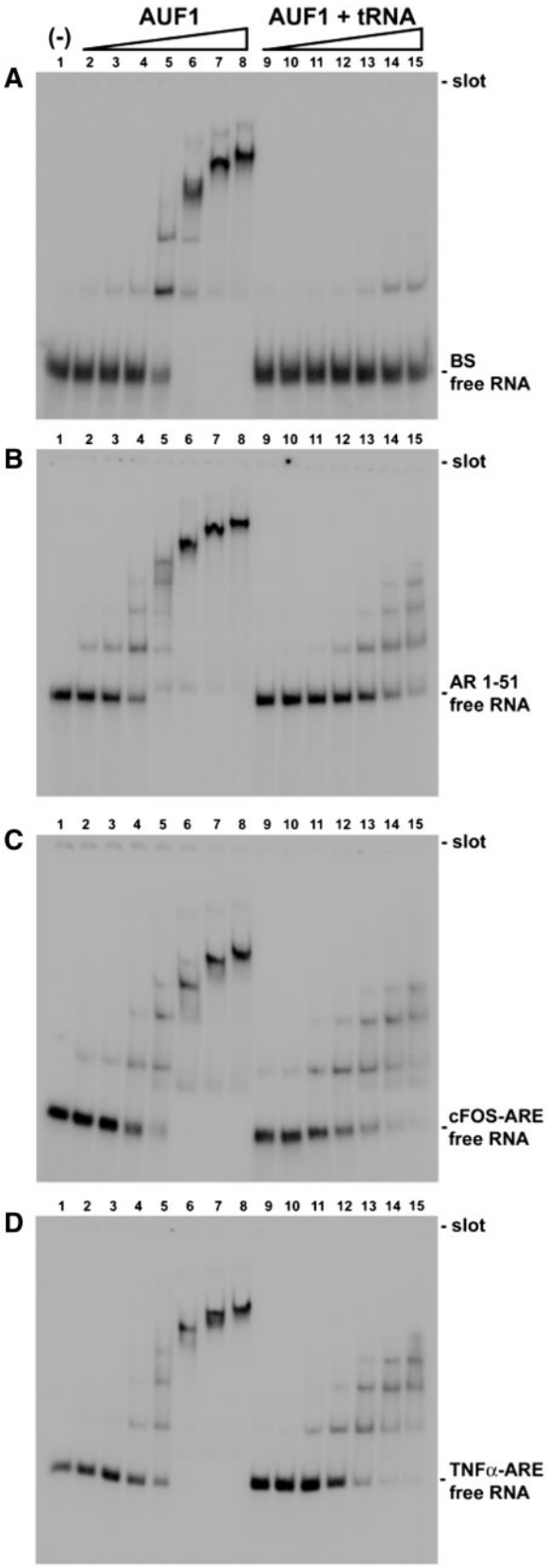

Fig. 6 AUF1 p37 binds to the AR 1–51 target sequence. REMSA gels are shown in which purified AUF1 interacts with: (A) BS (derived from empty vector); (B) AR 1–51 target RNA; (C) cFOS-ARE target RNA; or (D) TNFα-ARE either in the presence or absence of competitor tRNA. Labelling of the gels and protein and RNA concentrations are the same as previously.

that would instead be protected from RNaseT1 digestion if it were bound by HuR. RNaseV$_1$ digestion shows that the target sequence is partially double stranded under the experimental conditions used, but also that binding by HuR or HuR$_{I\&II}$ causes changes in this base pairing—in particular the increasing RNaseV$_1$ sensitivity with increasing concentrations of both proteins visible in the region 3′ of the protected bases (lanes 24–30). RNaseA digestion (lanes 3–9) confirms the results obtained with RNase1, although interpretation is complicated by the striking digestion pattern obtained. With this target RNA, RNaseA shows an almost exclusive preference for the distal uracil in a string of uracils, when they are interspersed with single adenines, as in the classical ARE sequence. The same digestion pattern was observed for RNaseA digestion of TNFα-ARE and cFOS-ARE (Supplementary Fig. S2) target RNAs.

Finally, we examined HuR and HuR$_{I\&II}$ binding to the MTA1 M1 target RNA using RNase footprint assays. Apart from alterations in digestion pattern caused by the U21G, U22G and U23G substitutions introduced in MTA1 M1, the digestion patterns obtained were indistinguishable from those shown in Fig. 9 (data not shown), confirming that HuR and HuR$_{I\&II}$ are interacting with the same target sequence in both target RNAs.

Discussion

Our analysis illustrates that the primary sequence feature in the *cis*-elements bound by HuR in the AR 3′-UTR and within the ARE elements present in the 3′-UTR of cFOS and TNFα mRNAs are their U-richness and single strandedness, as previously determined (*24*, *25*). Furthermore, we demonstrate that the HuR binding site within the 3′-UTR of MTA1 is not the motif suggested previously (*44*), but a sequence 3′ to that described, which is a classical ARE-type sequence (*24*, *25*). In particular, our results show that the sequence necessary for high-affinity binding by HuR is at least partially single stranded (to allow access of the individual RRM domains to the bases) and that two stretches of eight or nine uracils within an approximately 30 base region are necessary. Substitutions of some uracils with adenine (classical ARE) or cytosine (AR binding site) does not seem to affect affinity, but the presence of guanines does have a dramatic affect on HuR affinity for this sequence. These results are consistent with the crystal

Table IV. Apparent K_d values for the initial binding of AUF1 in the presence of competitor tRNA to AR 1–51, cFOS-ARE, TNFα-ARE or negative control (BS) target RNAs shown in Fig. 6.

	K_d (nM)
Target RNA	**AUF1**
AR 1–51	230 ± 130
cFOS-ARE	89 ± 11
TNFα-ARE	210 ± 40
BS	>1,000

structure for the first two RRM domains of the closely related HuD bound to two different target RNAs derived from cFOS-ARE or TNFα-ARE, which show specific contacts to U-rich sequences 8 or 9 bases long, respectively (*15*). We propose that these rules for HuR binding may more closely represent those active *in vivo* than the 17–20 base motif suggested elsewhere (*44*), and note that recent microarray- and PAR-CLIP-based approaches have led to a similar conclusion (*55–57*).

The striking digestion pattern obtained after RNaseA digestion of TNFα-ARE, cFOS-ARE and MTA1 target RNAs could be due to the specificity determinants of RNaseA, which prior to RNA hydrolysis binds to three adjacent bases with three discrete enzymatic subsites. Pyrimidine specificity is conferred by subsite B1, whereas subsite B2 prefers adenine and B3 prefers purine (*58*). Thus, the presence of an adjacent adenine (or guanine) immediately 3′ to the last uracil in each run of uracils in the MTA1, TNFα-ARE or cFOS-ARE could lead to the base preference observed, whereas the presence of an adjacent cytosine, as in the AR 1–51 target, would not lead to a heightened preference for the distal uracil.

The four AUF1 isoforms, generated from splice variants of AUF1 pre-mRNA, make it impossible to

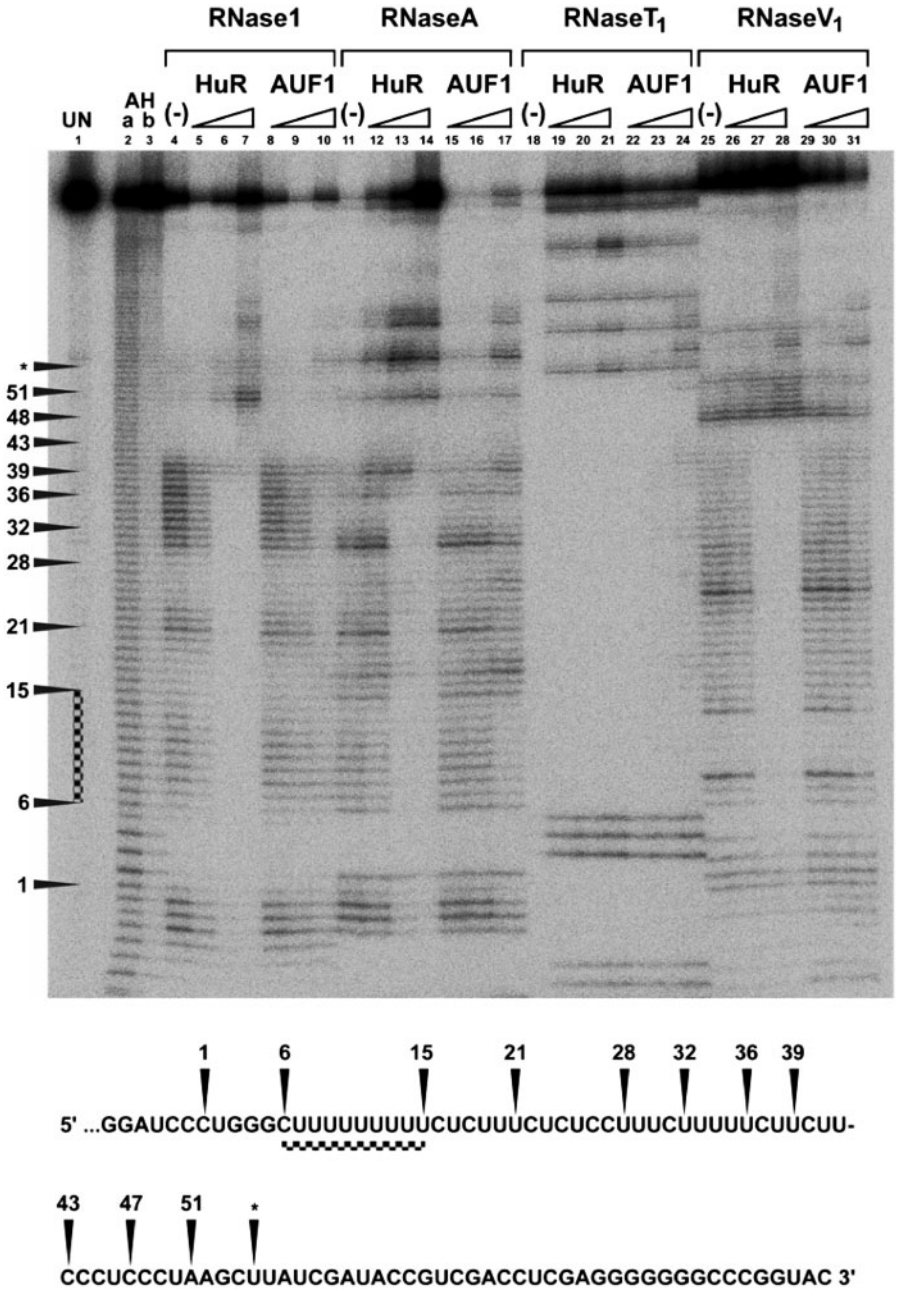

Fig. 7 AUF1 p37 and HuR bind to the same target sequence in AR 1–51 target RNA. Lane labelling and RNAse designations are identical to the gel shown in Fig. 5, except that the target RNA used is derived from Acc65I-linearized template (Supplementary Fig. S1). Protein concentrations are: 1×10^{-8} M; 1×10^{-7} M; or 1×10^{-6} M, instead of as indicated in Fig. 5. The asterisk at base U55 indicates the 3′-end of the probe used in Fig. 5.

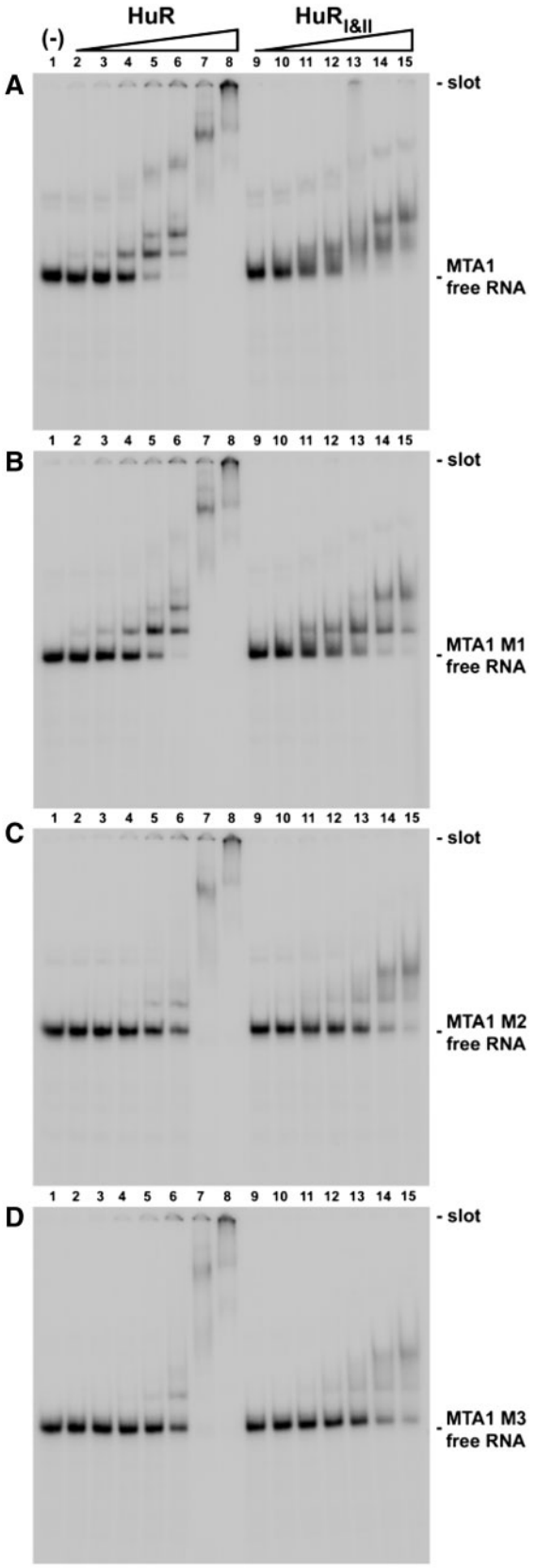

Fig. 8 Mutation of bases within the MTA1 target RNA shows that the HuR binding site is distinct from the predicted motif. REMSA gels are shown in which HuR or $HuR_{I\&II}$ interact with: (A) MTA1; (B) MTA1 M1; (C) MTA1 M2 or (D) MTA1 M3 target RNAs. Labelling of the gels and concentrations of HuR, $HuR_{I\&II}$ and target RNAs are the same as previously.

design siRNAs that are specific for a single isoform (*18*). In addition, AUF1 p37 has proved difficult to purify in a non-degraded form in our hands (data not shown) and the relatively low affinity of AUF1 p37 for AR 1–51 in comparison with the cFOS-ARE has precluded conducting a detailed analysis of the type presented here for HuR. Thus, we have not been able to examine the target sequence preference or competition for binding between HuR and AUF1 for the AR target site (*21*, *22*, *46*). AUF1 p40 phosphorylation outside of the RRM domains does influence the TNFα mRNA stability (*20*) but whether this is purely due to differences in the affinity of phosphorylated AUF1 p40 for the target RNA, the recruitment by phosphorylated AUF1 p40 of co-factors, or both, has not been determined. It is unlikely that protein phosphorylation *per se* will increase protein affinity for negatively charged RNA. Therefore, the issue of whether the two proteins do compete directly for the AR target sequence remains unanswered, although the fact that the same bases in the AR target examined here are protected from RNase digestion by both proteins, in addition to other results (*21*, *22*) is extremely suggestive.

Although our results have clarified the sequences actually contacted by HuR, three important points remain unanswered at this time. Although we can now identify bases contacted by HuR with confidence, whether a putative binding site is actually bound by HuR in a particular cell type is still a challenge. Although the RNA secondary structure predictions employed here are a useful indicator of RNA secondary structure *in vitro*, the formation of a comparable secondary structure in cells is more complex, and influenced by the presence or absence of multiple protein factors (*59*). Thus, even if a particular mRNA is bound by HuR in a particular cell type, it may not necessarily be bound in other cell types. Hence, an experimental approach to the positive identification of HuR targets will remain at the forefront of attempts to define its action under varying conditions.

Second, the stoichiometry of HuR–RNA complexes remains unclear. Examination of the crystal structure of the first two RRM domains of the related HuD bound to 11 base RNAs derived from the cFOS-ARE and TNFα-AREs examined here (*15*) supports our hypothesis that the initial binding event involves one monomer of HuR (or two monomers of $HuR_{I\&II}$) binding to one target RNA molecule. A comparable structure for HuR has not yet been reported, although

Table V. Apparent K_d values for the initial binding of HuR or $HuR_{I\&II}$ to MTA1 or target RNAs with substitution mutations shown in Fig. 8.

	K_d (nM)	
Target RNA	**HuR**	**$HuR_{I\&II}$**
MTA1	82 ± 16	86 ± 11
MTA1 M1	91 ± 17	130 ± 10
MTA1 M2	400 ± 220	370 ± 60
MTA1 M3	520 ± 370	500 ± 140

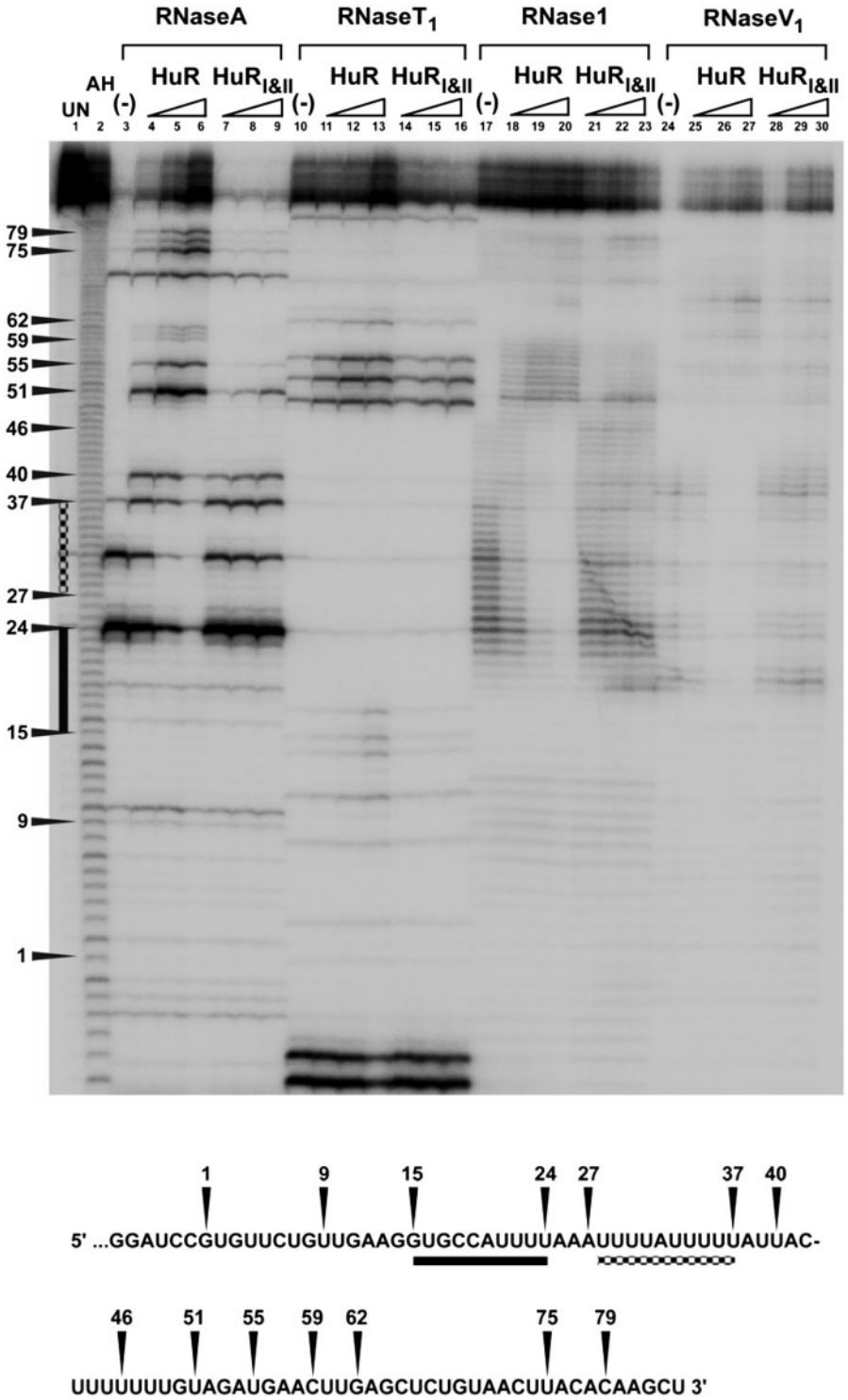

Fig. 9 RNase footprint analysis of HuR binding to MTA1 target RNA. Lane labelling, protein concentrations and RNase designations are identical to the gel shown in Fig. 5, except that the target RNA used is the MTA1 target RNA. The bases predicted to form the HuR binding site (*44*) are indicated by solid black lines in the target sequence and to the left of the gel, whereas the bases protected by the lowest concentrations of HuR or $HuR_{I\&II}$ are indicated by dashed lines.

a preliminary crystallization report has appeared (*60*). Our results indicate that the AR binding site can be dissected into a primary binding site and a secondary site, with binding to the entire site by at least two monomers of HuR occurring with higher affinity than binding of apparent monomers of HuR to the constituent minimal binding sites, thus raising the possibility of cooperativity between HuR monomers. Our analysis of binding to the MTA1 target site supports this through showing the binding of additional HuR distally to the first bound protein, although the experimental approach of adding increasing amounts of

protein could uncover secondary binding sites that are not contacted under normal, physiological conditions. Confirmation of our hypothesis, however, awaits a rigorous analysis using soluble protein.

Finally, the question remains as to the nature of the postulated motif identified elsewhere (*44*). Although our results show that the identified sequence is not directly contacted by HuR, the presence of such a highly conserved sequence in the region of so many mRNAs confirmed to be contacted by HuR is intriguing, particularly in the light of the recent observation of the requirement for HuR in the micro-RNA let-7-mediated destabilization of c-Myc mRNA (*61*). Firstly, the relative lack of an effect of site-specific mutations on reporter expression seen here indicates that sequences outside of the minimal HuR binding site contribute to the HuR-mediated stabilization of AR (*40*) and MTA1 (*44*) mRNAs. Second, examination of the motif sequences in the HuR targets (*44*) reveals that although a number of them do indeed contain predicted seed binding regions (*62*, *63*) for micro-RNAs (e.g. miR-505 in the MTA1 3′-UTR; and miR-412 in the FKBP1A 3′-UTR) others do not (e.g. the PTMA 3′-UTR) and even where the motif does contain a predicted micro-RNA seed they do not show a high degree of sequence similarity. Furthermore, some of the motif predictions lie within the coding region for a number of the mRNAs [including CRYZL1, the second motif we did not examine predicted (*44*) for MTA1, PP1CB, PVR and SUB1] and are therefore in any case unlikely to be involved with HuR binding to mature, translationally active mRNA. The function, if any, of this motif therefore remains unresolved.

Supplementary Data

Supplementary Data are available at *JB* online.

Acknowledgements

We are grateful to Gary Brewer for his generous gift of plasmid pBAD/HisB-p37AUF1.

Funding

Australian Research Council (Grant no. DP0345376) and National Health and Medical Research Council of Australia (Grant no. 353575).

Conflict of interest

None declared.

References

1. Doller, A., Pfeilschifter, J., and Eberhardt, W. (2008) Signalling pathways regulating nucleo-cytoplasmic shuttling of the mRNA-binding protein HuR. *Cell Signalling* **20**, 2165–2173
2. Laroia, G. and Schneider, R.J. (2002) Alternate exon insertion controls selective ubiquitination and degradation of different AUF1 protein isoforms. *Nucleic Acids Res.* **30**, 3052–3058
3. Wilson, G.M., Lu, J., Sutphen, K., Suarez, Y., Sinha, S., Brewer, B., Villanueva-Feliciano, E.C., Ysla, R.M., Charles, S., and Brewer, G. (2003) Phosphorylation of $p40^{AUF1}$ regulates binding to A + U-rich mRNA destabilizing elements and protein-induced changes in ribonucleoprotein structure. *J. Biol. Chem.* **278**, 33039–33048
4. Raineri, I., Wegmueller, D., Gross, B., Certa, U., and Moroni, C. (2004) Roles of AUF1 isoforms, HuR and BRF1 in ARE-dependent mRNA turnover studied by RNA interference. *Nucleic Acids Res.* **32**, 1279–1288
5. Good, P.J. (1995) A conserved family of *elav*-like genes in vertebrates. *Proc. Natl. Acad. Sci. USA* **92**, 4557–4561
6. Ma, W.-J., Cheng, S., Campbell, C., Wright, A., and Furneaux, H. (1996) Cloning and characterization of HuR, a ubiquitously expressed Elav-like protein. *J. Biol. Chem.* **271**, 8144–8151
7. Fan, X.C. and Steitz, J.A. (1998) HNS, a nuclear-cytoplasmic shuttling sequence in HuR. *Proc. Natl. Acad. Sci. USA* **95**, 15293–15298
8. Fan, X.C. and Steitz, J.A. (1998) Overexpression of HuR, a nuclear-cytoplasmic shuttling protein, increases the *in vivo* stability of ARE-containing mRNAs. *EMBO J.* **17**, 3448–3460
9. Atasoy, U., Watson, J., Patel, D., and Keene, J.D. (1998) ELAV protein HuA (HuR) can redistribute between nucleus and cytoplasm and is upregulated during serum stimulation and T cell activation. *J. Cell Sci.* **111**, 3145–3156
10. Kim, H.O., Yang, X., Kuwano, Y., and Gorospe, M. (2008) Modification at HuR(S242) alters HuR localization and proliferative influence. *Cell Cycle* **7**, 3371–3377
11. Kim, H.O., Abdelmohsen, K., Lal, A., Pullmann, R. Jr, Yang, X., Galban, S., Srikantan, S., Martindale, J.L., Blethrow, J., Shokat, K.M., and Gorospe, M. (2008) Nuclear HuR accumulation through phosphorylation by Cdk1. *Genes Dev.* **22**, 1804–1815
12. Chung, S., Jiang, L., Cheng, S., and Furneaux, H. (1996) Purification and properties of HuD, a neuronal RNA-binding protein. *J. Biol. Chem.* **271**, 11518–11524
13. Varani, G. and Nagai, K. (1998) RNA recognition by RNP proteins during RNA processing. *Ann. Rev. Biophys. Biomol. Struct.* **27**, 407–445
14. Park, S., Myszka, D.G., Yu, M., Littler, S.J., and Laird-Offringa, I.A. (2000) HuD RNA recognition motifs play distinct roles in the formation of a stable complex with AU-rich RNA. *Mol. Cell Biol.* **20**, 4765–4772
15. Wang, X. and Tanaka Hall, T.M. (2001) Structural basis for recognition of AU-rich element RNA by the HuD protein. *Nat. Struct. Biol.* **8**, 141–145
16. Ma, W.-J., Chung, S., and Furneaux, H. (1997) The ELAV-like proteins bind to AU-rich elements and to the poly(A) tail of mRNA. *Nucleic Acids Res.* **25**, 3564–3569
17. Meisner, N.-C., Hintersteiner, M., Seifert, J.-N., Bauer, R., Benoit, R.M., Widmer, A., Schindler, T., Uhl, V., Lang, M., Gstach, H., and Auer, M. (2009) Terminal adenosyl transferase activity of posttranscriptional regulator HuR revealed by confocal on-bead screening. *J. Mol. Biol.* **386**, 435–450
18. Wagner, B., DeMaria, C.T., Sun, Y., Wilson, G.M., and Brewer, G. (1998) Structure and genomic organization of the human AUF1 gene: alternative pre-mRNA splicing generates four protein isoforms. *Genomics* **48**, 195–202
19. Sarkar, B., Lu, J.-Y., and Schneider, R.J. (2003) Nuclear import and export functions in the different

isoforms of the AUF1/heterogeneous nuclear ribonucleoprotein protein family. *J. Biol. Chem.* **278**, 20700–20707

20. Wilson, G.M., Lu, J., Sutphen, K., Sun, Y., Huynh, Y., and Brewer, G (2003) Regulation of A + U-rich element-directed mRNA turnover involving reversible phosphorylation of AUF1. *J. Biol. Chem.* **278**, 33029–33038
21. Lal, A., Mazan-Mamczarz, K., Kawai, T., Yang, X., Martindale, J.M., and Gorospe, M. (2004) Concurrent versus individual binding of HuR and AUF1 to common labile target mRNAs. *EMBO J.* **23**, 3092–3102
22. David, P.S., Tanveer, R., and Port, D. (2007) FRET-detectable interactions between the ARE binding proteins, HuR and p37AUF1. *RNA* **13**, 1453–1468
23. Chen, C.Y. and Shyu, A.B. (1995) AU-rich elements: characterization and importance in mRNA degradation. *Trends Biochem. Sci.* **20**, 465–470
24. Barreau, C., Paillard, L., and Osborne, H.B. (2006) AU-rich elements and associated factors: are there unifying principles? *Nucleic Acids Res* **33**, 7138–7150
25. Meisner, N.-C., Hackermüller, J., Uhl, V., Aszódi, A., Jaritz, M., and Auer, M. (2004) nRNA openers and closers: modulating AU-rich element-controlled mRNA stability by a molecular switch in mRNA secondary structure. *Chem. Biochem.* **5**, 1432–1447
26. Gallouzi, I.E., Brennan, C.M., Stenberg, M.G., Swanson, M.S., Eversole, A., Maizels, N., and Steitz, J.A. (2000) HuR binding to cytoplasmic mRNA is perturbed by heat shock. *Proc. Natl. Acad. Sci. USA* **97**, 3073–3078
27. Brennan, C.M. and Steitz, J.A. (2001) HuR and mRNA stability. *Cell Mol. Life Sci.* **58**, 266–277
28. Galbán, S., Martindale, J.L., Mazan-Mamczarz, K., López de Silanes, I., Fan, J., Wang, W., Decker, J., and Gorospe, M. (2003) Influence of the RNA-binding protein HuR in pVHL-regulated p53 expression in renal carcinoma cells. *Cell Biol.* **23**, 7083–7095
29. Mazan-Mamczarz, K., Galbán, S., López de Silanes, I., Martindale, J.L., Atasoy, U., Keene, J.D., and Gorospe, M. (2003) RNA-binding protein HuR enhances p53 translation in response to ultraviolet light irradiation. *Proc. Natl. Acad. Sci. USA* **100**, 8354–8359
30. Katsanou, V., Papadaki, O., Milatsos, S., Blackshear, P.J., Anderson, P., Kollias, G., and Kontoyiannis, D.L. (2005) HuR as a negative posttranscriptional modulator in inflammation. *Mol. Cell* **19**, 777–789
31. Jeyaraj, S., Dakhlallah, D., Hill, S.R., and Lee, B.S. (2005) HuR stabilizes vacuolar H^+-translocating ATPase mRNA during cellular energy depletion. *J. Biol. Chem.* **280**, 37957–37964
32. Zou, T., Mazan-Mamczarz, K., Rao, J.N., Liu, L., Marasa, B.S., Zhang, A.-H., Xiao, L., Pullman, R., Gorospe, M., and Wang, J.-Y. (2006) Polyamine depletion increases cytoplasmic levels of RNA-binding protein HuR leading to stabilization of nucleophosmin and p53 mRNAs. *J. Biol. Chem.* **281**, 19387–19394
33. Figueroa, A., Cuadrado, A., Fan, J., Atasoy, U., Muscat, G.E., Munoz-Canoves, P., Gorospe, M., and Muñoz, A. (2003) Role of HuR in skeletal myogenesis through coordinate regulation of muscle differentiation genes. *Mol. Cell Biol.* **23**, 4991–5004
34. Gantt, K., Cherry, J., Tenney, R., Karschner, V., and Pekala, P.H. (2005) An early event in adipogenesis, the nuclear selection of the CCAAT enhancer-binding protein β (C/EBPβ) mRNA by HuR and its translocation to the cytosol. *J. Biol. Chem.* **280**, 24768–24774
35. Deschênes-Furry, J., Bélanger, G., Mwanjewe, J., Lunde, J.A., Parks, R.J., Perrone-Bizzozero, N., and Jasmin, B.J. (2005) The RNA-binding protein HuR binds to acetylcholinesterase transcripts and regulates their expression in differentiating skeletal muscle cells. *J. Biol. Chem.* **280**, 25361–25368
36. Hostetter, C., Licata, L.A., Witkiewicz, A., Costantino, C.L., Yeo, C.J., Brody, J.R., and Keen, J.C. (2008) Cytoplasmic accumulation of the RNA binding protein HuR is central to tamoxifen resistance in estrogen receptor positive breast cancer cells. *Cancer Biol. Ther.* **7**, 1496–1506
37. Mazan-Mamczarz, K., Hanger, P.R., Corl, S., Srikantan, S., Wood, W.H., Becker, K.G., Gorospe, M., Keene, J.D., Levenson, A.S., and Gartenhaus, R.B. (2008) Post-transcriptional gene regulation by HuR promotes a more tumorigenic phenotype. *Oncogene* **27**, 6151–6163
38. Niesporek, S., Kristiansen, G., Thoma, A., Weichert, W., Noske, A., Buckendahl, A.-C., Jung, K., Stephan, C., Dietl, M., and Denkert, C. (2008) Expression of the ELAV-like protein HuR in human prostate carcinoma is an indicator of disease relapse and linked to COX-2 expression. *Int. J. Oncol.* **32**, 341–347
39. Hasegawa, H., Kakuguchi, W., Kuroshima, T., Kitamura, T., Tanaka, S., Kitagawa, Y., Totsuka, Y., Shindoh, M., and Higashino, F. (2009) HuR is exported to the cytoplasm in oral cancer cells in a different manner from that of normal cells. *Br. J. Cancer* **100**, 1943–1948
40. Yeap, B.B., Voon, D.C., Vivian, J.P., McCulloch, R.K., Thomson, A.M., Giles, K.M., Czyzyk-Krzeska, M.F., Furneaux, H., Wilce, M.C.J., Wilce, J.A., and Leedman, P.J. (2002) Novel binding of HuR and poly(C)-binding protein to a conserved UC-rich motif within the 3′-untranslated region of the androgen receptor messenger RNA. *J. Biol. Chem.* **277**, 27183–27192
41. Sheflin, L.G., Zou, A.-P., and Spaulding, S.W. (2004) Androgens regulate the binding of endogenous HuR to the AU-rich 3′UTRs of HIF-1α and EGF mRNA. *Biochem. Biophys. Res. Commun.* **322**, 644–651
42. Arao, Y., Kikuchi, A., Kishida, M., Yonekura, M., Inoue, A., Yasuda, S., Wada, S., Ikeda, K., and Kayama, F. (2004) Stability of A + U-rich element binding factor 1 (AUF1)-binding messenger ribonucleic acid correlates with the subcellular relocalization of AUF1 in the rat uterus upon estrogen treatment. *Mol. Endocrinol.* **18**, 2255–2267
43. Sheflin, L.G. and Spaulding, S.W. (2000) Testosterone and dihydrotestosterone regulate AUF1 isoforms in a tissue-specific fashion in the mouse. *Am. J. Physiol. Endocrinol. Metab.* **278**, E50–E57
44. López de Silanes, I., Zhan, M., Lal, A., Yang, X., and Gorospe, M. (2004) Identification of a target RNA motif for RNA-binding protein HuR. *Proc. Natl. Acad. Sci. USA* **101**, 2987–2992
45. Westmark, C. J., Gourronc, F.A., Bartleson, V.B., Sayin, U., Bhattacharya, S., Sutula, T., and Malter, J.S. (2005) HuR mRNA ligands expressed after seizure. *J. Neuropathol. Exp. Neurol.* **64**, 1037–1045
46. Mazan-Mamczarz, K., Kuwano, Y., Zhan, M., White, E.J., Martindale, J.L., Lal, A., and Gorospe, M. (2009) Identification of a signature motif in target mRNAs of RNA-binding protein AUF1. *Nucleic Acids Res.* **37**, 204–214

47. Wilson, G.M., Sutphen, K., Chuang, K., and Brewer, G. (2001) Folding of A + U rich RNA elements modulates AUF1 binding: potential roles in regulation of mRNA turnover. *J. Biol. Chem.* **276**, 8695–8704
48. Giles, K.M., Daly, J.M., Beveridge, D.J., Thomson, A.M., Voon, D.C., Furneaux, H.M., Jazayeri, J.A., and Leedman, P.J. (2003) The 3′-untranslated region of $p21^{WAF1}$ mRNA is a composite *cis*-acting sequence bound by RNA-binding proteins from breast cancer cells, including HuR and poly(C)-binding protein. *J. Biol. Chem.* **278**, 2937–2946
49. Miller, J. (1972) *Experiments in Molecular Genetics*. Cold Spring Harbor Laboratory Press, Cold Spring Harbor, NY
50. Gasteiger, E., Gattiker, A., Hoogland, C., Ivanyi, I., Appel, R.D., and Bairoch, A. (2003) ExPASy: the proteomics server for in-depth protein knowledge and analysis. *Nucleic Acids Res.* **31**, 3784–3788
51. Zuker, M. (2003) Mfold web server for nucleic acid folding and hybridization prediction. *Nucleic Acids Res.* **31**, 3406–3415
52. Oehler, S., Alex, R., and Barker, A. (1999) Is nitrocellulose filter binding really a universal assay for protein-DNA interactions? *Anal. Biochem.* **268**, 330–336
53. Soller, M. and White, K. (2005) ELAV multimerizes on conserved AU_{4-6} motifs important for *ewg* splicing regulation. *Mol. Cell Biol.* **25**, 7580–7591
54. Wilson, G.M., Sun, Y., Lu, H., and Brewer, G. (1999) Assembly of AUF1 oligomers on U-rich RNA targets by sequential dimer association. *J. Biol. Chem.* **274**, 33374–33381
55. Ray, D., Kazan, H., Chan, E.T., Castillo, L.P., Chaudhry, S., Talukder, S., Blencowe, B.J., Morris, Q., and Hughes, T.R. (2009) Rapid and systematic analysis of the RNA recognition specificities of RNA-binding proteins. *Nat. Biotech.* **27**, 667–670
56. Mukherjee, N., Corcoran, D.L., Nusbaum, J.D., Reid, D.W., Georgiev, S., Hafner, M., Ascano, M., Tuschl, T., Ohler, U., and Keene, J.D. (2011) Integrative regulatory mapping indicates that the RNA-binding protein HuR couples pre-mRNA processing and mRNA stability. *Mol. Cell* **43**, 327–339
57. Lebedeva, S., Jens, M., Theil, K., Schwanhausser, B., Selbach, M., Landthaler, M., and Rajewsky, N. (2011) Transcriptome-wide analysis of regulatory interactions of the RNA-binding protein HuR. *Mol. Cell* **43**, 340–352
58. delCardayré, S.B. and Raines, R.T. (1994) Structural determinants of enzymatic processivity. *Biochemistry* **33**, 6031–6037
59. Mahen, E.M., Harger, J.W., Calderon, E.M., and Fedor, M.J. (2005) Kinetics and thermodynamics make different contributions to RNA folding in vitro and in yeast. *Mol. Cell* **19**, 27–37
60. Iyaguchi, D., Yao, M., Tanaka, I., and Toyota, E. (2009) Cloning, expression, purification and preliminary crystallographic studies of the adenylate/uridylate-rich element-binding protein HuR complexed with its target RNA. *Acta Crytallogr. Sect. F Struct. Biol. Cryst. Commun.* **65**, 285–287
61. Kim, H.H., Kuwano, Y., Srikantan, S., Lee, E.K., Martindale, J.L., and Gorospe, M. (2009) HuR recruits let-7/RISC to repress c-Myc expression. *Genes Dev.* **23**, 1743–1748
62. Lewis, B.P., Shih, I.-H., Jones-Rhoades, M.W., Bartel, D.P., and Burge, C.B. (2003) Prediction of mammalian microRNA targets. *Cell* **115**, 787–798
63. Lewis, B.P., Burge, C.B., and Bartel, D.P. (2005) Conserved seed pairing, often flanked by adenosines, indicates that thousands of human genes are microRNA targets. *Cell* **120**, 15–20